Reduction of SINR Fluctuation in Indoor Multi-Cell VLC Systems Using Optimized Angle Diversity Receiver

Chen Chen, Wen-De Zhong, *Senior Member, IEEE*, Helin Yang, Sheng Zhang, and Pengfei Du

***Abstract*—Due to severe inter-cell interference (ICI), the signal-to- interference-and-noise ratio (SINR) suffers from very significant fluctuation in indoor multi-cell visible light communication (VLC) systems, which greatly limits the overall system performance. In this paper, we propose and evaluate a generalized angle diversity receiver (ADR) structure to reduce SINR fluctuation in indoor multi-cell VLC systems. The generalized ADR consists of one top detector and multiple inclined side detectors. In an indoor multi-cell VLC system using the generalized ADR, the inclination angle of the side detectors is optimized in order to minimize the SINR fluctuation over the receiving plane, where the impact of receiver random rotation is considered. An optimized ADR with different numbers of detectors is analyzed with different LED layouts and diversity combining techniques in a typical indoor environment. Analytical results show that the SINR fluctuation is gradually reduced when more detectors are equipped in the optimized ADR. In an indoor two-cell VLC system, much more significant SINR fluctuation reduction is achieved by using select-best combining (SBC). However, nearly the same SINR fluctuations are obtained in an indoor four-cell VLC system when using SBC and maximal-ratio combining (MRC). By applying the optimized ADR, up to 15.9 and 32.4-dB SINR fluctuation reductions can be achieved in comparison to a conventional single-element receiver (SER) in indoor two-cell and four-cell VLC systems, respectively.**

***Index Terms*—Angle diversity receiver (ADR), multi-cell, optimization, SINR fluctuation, visible light communication (VLC).**

I. Introduction

THERE has been ever-increasing research interest in visible light communication (VLC) in recent years, due to the rapid development of light-emitting diode (LED) technology. It is anticipated that LEDs will gradually replace incandescent and fluorescent lamps for indoor illumination and dominate the illumination market by 2020 [1]. Besides illumination, LEDs can also be used for high-speed data communication in indoor environments [2]. White LEDs enabled VLC has been viewed as a promising complementary technology to radio-frequency (RF) technologies [3]. By exploiting high-speed, bidirectional and networked VLC systems, light-fidelity (Li-Fi) can be deployed in typical indoor environments [4], which exhibits inherent advantages compared with the widely used wireless-fidelity (Wi-Fi), such as unregulated spectrum, potentially high data rate, low-cost front-ends and electromagnetic interference-free operation [5]. Besides communication, LEDs based VLC also has many other emerging applications such as positioning, sensing, object ranging and detecting, and so on [6]–[8].

Due to the long photoluminescence lifetime of phosphor in LEDs, the 3-dB modulation bandwidth of off-the-shelf white LEDs is only about a few MHz, which significantly limits the capacity of VLC systems [9]. So far, a lot of techniques have been proposed to increase the capacity of white LEDs based VLC systems, for example, equalization techniques including digital/analog frequency domain equalization at transmitter or receiver [10], [11], spectral-efficient modulation schemes such as orthogonal frequency division multiplexing (OFDM) [12], [13], multiple-input multiple-output (MIMO) [14], [15], power domain non-orthogonal multiple access (NOMA) [16], [17], etc. Nevertheless, the focus of most existing works is mainly on the capacity improvement of single-cell VLC systems.

In practical indoor environments, a VLC system is usually composed of multiple small cells, i.e., optical attocells, such that full communication coverage of an indoor environment can be achieved [18]. It has been shown in many studies that inter-cell interference (ICI) is a major issue that severely degrades the overall performance of an indoor multi-cell VLC system [18], [19]. When users are located at the overlapping area of adjacent cells, the signal-to-interference-and-noise ratio (SINR) of these users would be considerably low due to the existence of strong interference. In order to efficiently mitigate the ICI and hence improve the overall performance of multi-cell VLC systems, several approaches have been reported in recent years. Kim *et al.* demonstrated a frequency division based carrier allocation approach in [20], where different RF subcarriers are allocated to different cells and electrical filtering is used to extract the desired RF subcarrier for each cell. Although the ICI can be efficiently mitigated, the achievable spectral efficiency within each cell is substantially reduced due to spectrum partitioning and the use of a large guard band (GB). An improved carrier allocation approach using filter bank multicarrier (FBMC) was further proposed in [21], where the GB is greatly

Manuscript received January 19, 2018; revised May 23, 2018; accepted May 27, 2018. Date of publication May 30, 2018; date of current version July 12, 2018. This work was supported by Delta Electronics Inc. and the National Research Foundation (NRF) Singapore under the Corp Lab@University Scheme. *(Corresponding author: Chen Chen.)*

The authors are with the School of Electrical and Electronic Engineering, Nanyang Technological University, Singapore 639798 (e-mail: chen0884@e.ntu.edu.sg; ewdzhong@ntu.edu.sg; HYANG013@e.ntu.edu.sg; szhang034@e.ntu.edu.sg; PFDU@ntu.edu.sg).

Color versions of one or more of the figures in this paper are available online at http://ieeexplore.ieee.org.

Digital Object Identifier 10.1109/JLT.2018.2842080

reduced due to the suppressed spectrum sidelobes of FBMC. Nevertheless, the spectral efficiency improvement achieved by reducing the GB is limited since spectrum partitioning is still required. In [22], Bykhovsky and Arnon investigated a dynamic interference-constrained subcarrier reuse algorithm for OFDM based VLC in a heuristic manner, leading to an improvement in average bit-rate, but with a relatively high implementation complexity. In [23], Ryoo *et al.* demonstrated a differential optical detection approach based on polarization division, which could reduce in-band interference and hence avoid spectrum partitioning. However, accurate polarization control and cell planning are required to successfully implement this approach.

Recently, angle diversity receivers (ADRs) were introduced for improving the performance of indoor MIMO-VLC systems, since ADRs can efficiently decorrelate the optical channel and hence achieve high rank of channel matrix [24]–[26]. Optical receivers utilizing photodetectors with different fields of view were further applied to reduce channel correlation in MIMO-VLC systems [27], [28]. Moreover, ADRs were also employed to mitigate ICI in indoor multi-cell VLC systems, where all the detectors in each ADR are attached to a fixed semi-sphere base [29], [30]. However, the structures of ADRs are not optimized and therefore the resultant performance gain is still not yet fully exploited. In addition, the purpose of applying ADRs in indoor multi-cell VLC systems is only to increase the overall system capacity or the area spectral efficiency (ASE), while the SINR fluctuation over the receiving plane has not yet been studied. In our previous work [31], the performance of an indoor multi-cell VLC system using an ADR has been analyzed, where the ADR is optimized to achieve maximum SINR at the central position of an indoor four-cell VLC system. However, the optimization is only performed with respect to a single position in the system and the system-level optimization has not yet been investigated.

In this paper, we first propose a generalized ADR structure which consists of one top detector and multiple inclined side detectors, and the inclination angle of the side detectors can be adjusted. After that, from the user fairness point of view, we further perform a multi-parameter optimization to minimize the SINR fluctuation over the receiving plane of indoor multi-cell VLC systems. Although the work in [32] reported the signal-to-noise ratio (SNR) fluctuation reduction in an indoor single-cell VLC system through optimal arrangement of LEDs, to our best knowledge, it is the first time that SINR fluctuation reduction is examined in multi-cell VLC systems using an optimized ADR. The main contributions of this work are summarized as follows:

- A generalized ADR structure is proposed, consisting of one top detector and multiple inclined side detectors, which is scalable in the number of side detectors and flexible in the inclination angle of side detectors.
- A multi-parameter optimization is performed which aims to minimize the SINR fluctuation over the receiving plane and hence to improve user fairness in a multi-cell VLC system within a specific indoor environment, where various system parameters are taken into consideration such as the number and the inclination angle of the side detectors in the generalized ADR, the number of LED transmitters in the ceiling and the adopted diversity combining technique.
- The impact of receiver random rotation is considered in the optimization by evaluating the average SINR performance under the assumption that the rotation angle is uniformly distributed between 0° and 360° and further defining the SINR fluctuation as the difference between the highest and the lowest average SINRs over the receiving plane of an indoor multi-cell VLC system.

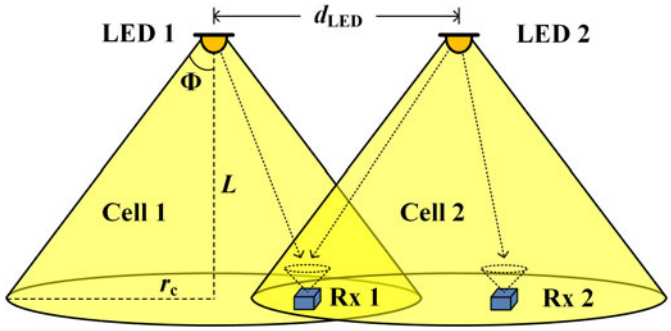

Fig. 1. Illustration of a multi-cell VLC system with inter-cell interference (ICI).

The rest of this paper is organized as follows. Section II presents the mathematical model of a multi-cell VLC system with ICI. In Section III, the principle of the generalized ADR is introduced. The optical channel gain and the SINR expressions are further derived. The results are provided in Section IV, and finally the conclusion and future work are given in Section V.

II. System Model

In this section, we present the mathematical model of an indoor multi-cell VLC system. As illustrated in Fig. 1, the LED light modulated with data is transmitted into free space for both illumination and wireless communication in typical indoor environments. Usually, there are two types of light components that can be received by a photodetector: one is a line-of-sight (LOS) component and the other is the diffuse component due to signal reflections from the surfaces within the room. Some previous work has shown that the strongest diffuse component is much lower in electrical power than the LOS component in typical indoor environments [9], [14]. Hence, it is reasonable to only consider the LOS component in the performance study of indoor multi-cell VLC systems.

The LOS irradiance of an LED can be assumed to follow a generalized Lambertian pattern [2]. Let N_t be the number of the LEDs in the ceiling and N_r be the number of the detectors in the receiver. The LOS optical channel gain between the *i*-th ($i = 1, 2, \ldots, N_t$) LED and the *j*-th ($j = 1, 2, \ldots, N_r$) detector in the receiver is calculated by

$$h_{ij} = \frac{(m+1)A_d}{2\pi d_{ij}^2} \cos^m(\varphi_{ij}) T(\theta_{ij}) g(\theta_{ij}) \cos(\theta_{ij}), \quad (1)$$

where $m = -\ln 2/\ln(\cos\Phi)$ is the order of Lambertian emission with Φ being the semi-angle at half power of each LED, A_d is

the active area of each detector, d_{ij} is the distance between the *i*-th LED and the *j*-th detector, φ_{ij} is the emission angle, θ_{ij} is the incident angle, $T(\theta_{ij})$ is the gain of the optical filter, and $g(\theta_{ij})$ is the gain of the optical concentrator which can be calculated by $g(\theta_{ij}) = n^2/\sin^2\Psi$, where n and Ψ are the refractive index and the half-angle field-of-view (FOV) of the optical concentrator, respectively. Note that h_{ij} becomes zero when the incident angle is larger than the FOV of the *j*-th detector.

After free-space propagation, the received electrical signal at the output of the *j*-th detector can be represented by

$$y_j(t) = \sum_{i=1}^{N_t} \gamma \xi h_{ij} P_0 x_i(t) + n_j(t), \tag{2}$$

where γ is the responsivity of the detectors, ξ is the modulation index of each LED, h_{ij} is the optical channel gain defined in (1), P_0 is the average output optical power of each LED, $x_i(t)$ is the transmitted electrical signal with unity power from the *i*-th LED, and $n_j(t)$ is the additive noise which includes the shot noise and the thermal noise. Both the shot and thermal noises can be modeled as real-valued additive white Gaussian noises (AWGNs) and their corresponding variances are given by

$$\begin{cases} \sigma^2_{j,\,shot} = 2q(\gamma P_j + I_{bg} I_2) B_n \\ \sigma^2_{j,\,thermal} = 8\pi k T_K \eta A B_n^2 \left(\frac{I_2}{G} + \frac{2\pi\Gamma}{g_m} \eta A_d I_3 B_n \right) \end{cases}, \tag{3}$$

where $P_j = P_0 \sum_{i=1}^{N_t} h_{ij}$ is the total received optical power from the N_t LEDs, I_{bg} is the background current due to ambient light, and B_n is the equivalent noise bandwidth. The other parameters shown in (3) can be found in [2].

Fig. 1 illustrates an indoor multi-cell VLC system which suffers from ICI, where only two adjacent cells are shown. In order to achieve full coverage of an indoor environment, there is always overlapping between the covered areas of adjacent cells. Thus, ICI is inevitable in indoor multi-cell VLC systems. As shown in Fig. 1, the distance between two adjacent LEDs (LED 1 and LED 2) is d_{LED}, the semi-angle at half power of each LED is Φ, and the height from the ceiling to the horizontal receiving plane is *L*. Each of two adjacent cells (cell 1 and cell 2) covers a circular area with a radius of $r_c = L \times \tan\Phi$. Hence, the ICI occurs when $d_{\text{LED}} < 2r_c$. It can be seen that there are two receivers (Rxs) corresponding to two users located in the room. Suppose that Rx 1 is served by cell 1 but located at the overlapping area of cell 1 and cell 2, while Rx2 is served by cell 2 and located at the non-overlapping area in cell 2. Then, Rx1 receives ICI from cell 2 while Rx2 is not affected by the ICI. For the Rx located at the non-overlapping area of a cell, it is served by its corresponding cell. However, for the Rx located at the overlapping area of adjacent cells, a specific cell that serves this Rx is usually selected based on the highest SINR [30].

Assuming that the *j*-th detector is served by the *i*-th LED, the SINR at the output of the *j*-th detector of the receiver can be expressed by

$$SINR_{ij} = \frac{(\gamma \xi h_{ij} P_0)^2}{\sum_{i'=1,\, i' \neq i}^{N_t} (\gamma \xi h_{i'j} P_0)^2 + \sigma^2_{j,\,shot} + \sigma^2_{j,\,thermal}}, \tag{4}$$

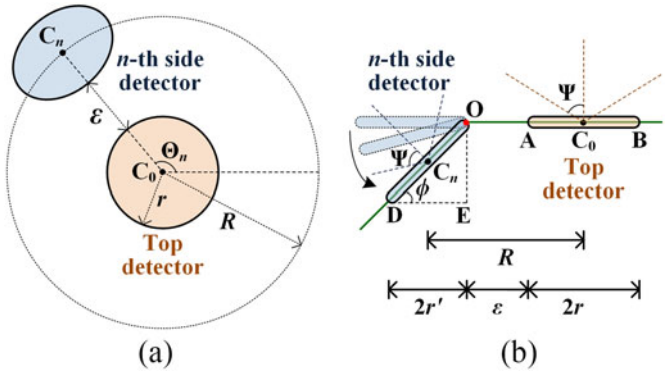

Fig. 2. (a) Top view and (b) side view of the proposed generalized ADR. Only the top detector and the *n*-th side detector are shown for illustration.

where $\sum_{i'=1,i' \neq i}^{N_t} (\gamma \xi h_{i'j} P_0)^2$ represents the electrical power of the interference signal from all the interfering LEDs, and $\sigma^2_{j,shot}$ and $\sigma^2_{j,thermal}$ are the noise variances defined in (3).

III. Generalized Angle Diversity Receiver

In order to reduce SINR fluctuation in indoor multi-cell VLC systems, a generalized ADR structure is proposed in this work.

A. Principle

The proposed generalized ADR structure consists of totally N_r circular-shaped detectors (elements), which includes one top detector and $N_r - 1$ inclined side detectors. All the detectors in the generalized ADR are assumed to have the same radius *r*, the same half-angle FOV Ψ and the same optical and electrical performance. The top view and the side view of the generalized ADR are depicted in Figs. 2(a) and (b), respectively. As shown in Fig. 2(a), the top detector is located at the central position C_0, while all the side detectors are located at the circumference of a circle which is centered at C_0 with a radius of *R*. The gap between the top detector and the side detector is ε. The azimuth angle of the *n*-th side detector is Θ_n. For the generalized ADR with N_r ($N_r \geq 3$) detectors, we assume that the azimuth angle of the 1-st side detector is fixed at $\Theta_1 = 0^\circ$ and hence the azimuth angle of the *n*-th side detector is represented by

$$\Theta_n = 360^\circ \times \frac{n-1}{N_r - 1},\ n = 2, \ldots,\ N_r - 1. \tag{5}$$

For example, when $N_r = 5$, the azimuth angles of all four side detectors are 0°, 90°, 180° and 270°. Fig. 2(b) shows the side view of the top detector and the *n*-th side detector. As we can see, the top detector is not inclined while the side detector is inclined. In the generalized ADR, all side detectors are assumed to have the same inclination angle ϕ. When the receiver is vertically oriented, the inclination angle of the *n*-th detector is expressed by

$$\phi_n = \begin{cases} 0^\circ, & \text{if } n = 0 \\ \phi, & \text{if } n = 1, \ldots,\ N_r - 1 \end{cases}. \tag{6}$$

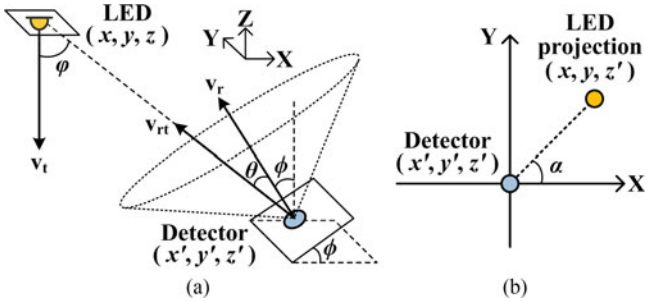

Fig. 3. (a) Geometry for optical channel gain calculation of the side detectors and (b) LED projection on the detector plane.

By rotating the side detector around the point O, as in Fig. 2(b), the inclination angle ϕ of the side detectors can be adjusted.

B. Optical Channel Gain

In the analysis throughout this paper, we assume that the receiver is vertically oriented and the position of the receiver is represented by the central position C_0 of the top detector. The impact of receiver tilting is beyond the scope of this paper. Based on the receiver geometry shown in Fig. 2, the relations between the position of the top detector and the positions of the side detectors can be derived. The radius *R*, i.e., the horizontal distance between C_0 and C_n, is calculated by $R = \varepsilon + r + r'$ and r' is given by $r' = r\cos\varphi$. Hence, we have $R = \varepsilon + r(1 + \cos\phi)$. Let $(x_0,\ y_0,\ z_0)$ and $(x_n,\ y_n,\ z_n)$ be the coordinates of positions C_0 and C_n, respectively. After some geometric calculations, we can get the relationship between $(x_0,\ y_0,\ z_0)$ and $(x_n,\ y_n,\ z_n)$:

$$\begin{cases} x_n = x_0 + [\varepsilon + r(1 + \cos\phi)]\cos\Theta_n \\ y_n = y_0 + [\varepsilon + r\,(1 + \cos\phi)]\,\sin\Theta_n \\ z_n = z_0 - r\sin\phi \end{cases}. \tag{7}$$

The optical channel gain of the uninclined top detector can be obtained by (1). However, the optical channel gain of a side detector cannot be directly calculated using (1), since all side detectors are inclined with a common inclination angle and each side detector is also rotated with its own azimuth angle.

Fig. 3(a) illustrates the geometry for the optical channel gain calculation of the side detectors. As can be seen, the emission angle φ is only determined by the positions of the LED and each side detector. Assuming that the LED and the side detector are located at (*x*, *y*, *z*) and (*x'*, *y'*, *z'*) respectively, we have

$$\cos\varphi = \frac{z - z'}{\left[(x - x')^2 + (y - y')^2 + (z - z')^2\right]^{1/2}}. \tag{8}$$

However, the incident angle θ is determined not only by the positions of the LED and the side detector, but also the inclination angle ϕ and the azimuth angle α. Taking the impact of receiver random rotation into consideration, the azimuth angle of the side detector is given by

$$\alpha = \Theta + \omega, \tag{9}$$

where Θ is the initial azimuth angle of the side detector without rotation, as defined in (5), and ω is the random rotation angle which is the same for all the side detectors and can be assumed to be uniformly distributed between 0° and 360° [33]. Let $\mathbf{v}_{\rm r}$ and $\mathbf{v}_{\rm rt}$ be the normal vector of the plane of the side detector and the vector from the side detector to the LED, respectively, we have

$$\cos\theta = \frac{(\mathbf{v}_{\rm r}, \mathbf{v}_{\rm rt})}{\|\mathbf{v}_{\rm r}\| \cdot \|\mathbf{v}_{\rm rt}\|}, \tag{10}$$

where $(\cdot,\cdot)$ denotes the inner product of two vectors and $\|\cdot\|$ is the vector norm. For a detector with an inclination angle ϕ and an azimuth angle α, the normal vector of the detector plane is given by [34]

$$\mathbf{v}_{\rm r} = [\sin\phi\cos\alpha, \sin\phi\sin\alpha, \cos\phi]\,. \tag{11}$$

The azimuth angle α of the side detector is determined by the positions of the LED projection and the side detector, as shown in Fig. 3(b), which is calculated by [35]

$$\alpha = \begin{cases} \alpha_0, & \text{if } x \geq x',\ y \geq y' \\ \pi - \alpha_0, & \text{if } x < x',\ y \geq y' \\ \pi + \alpha_0, & \text{if } x < x',\ y < y' \\ 2\pi - \alpha_0, & \text{if } x \geq x',\ y < y' \end{cases}, \tag{12}$$

where $\alpha_0 = arctan(|\,y - y'|/|x - x'|)$. Moreover, the vector from the side detector to the LED is expressed by

$$\mathbf{v}_{\rm rt} = [x,\ y,\ z] - [x',\ y',\ z'] = [x - x',\ y - y',\ z - z']\,. \tag{13}$$

Therefore, we can rewrite (10) as

$$\cos\theta = \frac{[(x - x')\cos\alpha + (y - y')\sin\alpha]\sin\phi + (z - z')\cos\phi}{\sqrt{(x - x')^2 + (y - y')^2 + (z - z')^2}}. \tag{14}$$

By substituting (8) and (14) into (1), we can obtain the optical channel gain for the side detector as shown in (15) at the bottom of this page. As we can see from (15), $h'(\phi)$ is a function of the inclination angle ϕ of the side detectors, which can be further optimized to achieved optimal performance.

C. SINR Analysis

Since the FOVs of two or more detectors in the generalized ADR might overlap with each other, multiple detectors might receive the desired signal for its serving cell simultaneously.

$$h'(\phi) = \begin{cases} \frac{(m+1)A_d T(\theta) g(\theta)\{[(x-x')\cos\alpha + (y-y')\sin\alpha]\sin\phi + (z-z')\cos\phi\}(z-z')^m}{2\pi d^2\left[(x-x')^2 + (y-y')^2 + (z-z')^2\right]^{(1+m)/2}}, & \text{if } \varphi \leq \Phi \text{ and } \theta \leq \Psi \\ 0, & \text{if } \varphi > \Phi \text{ or } \theta > \Psi \end{cases}. \tag{15}$$

To achieve a final output signal from multiple received signals, diversity combining can be adopted. In the following analysis, three different diversity combining techniques are investigated, including equal-gain combining (EGC), select-best combining (SBC) and maximal-ratio combining (MRC) [36].

The EGC is the simplest combination technique whereby all the output signals from N_r detectors are directly added with equal weights. Hence, the SINR of the combined signal using EGC can be calculated by

$$\lambda_{i,EGC} = \frac{\left(\sum_{j=1}^{N_r} \gamma\xi h'_{ij} P_0\right)^2}{\sum_{j=1}^{N_r}\left(\sum_{i'=1,\, i'\neq i}^{N_t} \left(\gamma\xi h'_{i'j} P_0\right)^2 + \sigma^2_{j,\,shot} + \sigma^2_{j,\,thermal}\right)}. \tag{16}$$

For the SBC technique, the output signal which achieves the highest SINR is selected as the final output signal. As a result, the SINR using SBC is given by

$$\lambda_{i,SBC} = \max_j (SINR'_{ij}) = \max_j \left(\frac{\left(\gamma\xi h'_{ij} P_0\right)^2}{\sum_{i'=1,\, i'\neq i}^{N_t} \left(\gamma\xi h'_{i'j} P_0\right)^2 + \sigma^2_{j,\,shot} + \sigma^2_{j,\,thermal}}\right), \tag{17}$$

where $SINR'_{ij}$ is the SINR at the output of the *j*-th detector of the generalized ADR serving by the *i*-th LED.

When adopting MRC, all the output signals are combined. Before combining, each output signal is first multiplied by a weight equal to its own SINR, i.e., $\omega_{ij} = SINR'_{ij}$. Therefore, the SINR of the combined signal using MRC can be expressed by (18) as shown at the bottom of this page.

As can be seen from (9), the azimuth angle of each side detector is determined by its initial azimuth angle and the common random rotation angle of the generalized ADR. To take the impact of receiver random rotation into consideration, we take average SINR as the merit to evaluate the performance of multi-cell VLC systems. It is assumed that the generalized ADR is randomly rotated for totally *M* times and the rotation angle ω_m ($m = 1, 2, \ldots, M$) is uniformly distributed between 0° and 360°. Denoting the SINR as λ_m when the rotation angle is ω_m, the average SINR is represented by

$$\bar{\lambda} = \frac{1}{M}\sum_{m=1}^{M} \lambda_m. \tag{19}$$

Substituting (16), (17) and (18) into (19) yields the average SINR using EGC, SBC and MRC, respectively.

Assuming there are totally *K* users located at the receiving plane of an indoor multi-cell VLC system and denoting the average SINR of the *k*-th ($k = 1, 2, \ldots, K$) user as $\bar{\lambda}_k$, the SINR fluctuation can be obtained by

$$\bar{\lambda} = \max_k (\bar{\lambda}_k) - \min_k (\bar{\lambda}_k). \tag{20}$$

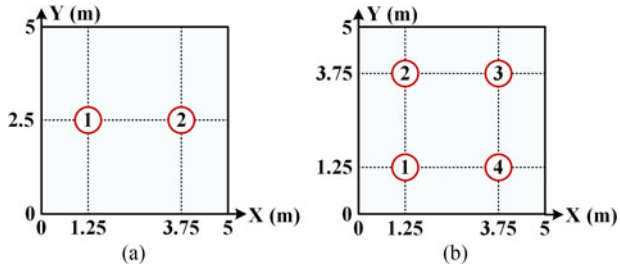

Fig. 4. LED layout in the ceiling with (a) $N_t = 2$ and (b) $N_t = 4$.

TABLE I
KEY PARAMETERS OF THE MULTI-CELL VLC SYSTEM

Parameter	Value
Room dimension (length × width × height)	5 m × 5 m × 3 m
Height of receiving plane	0.85 m
Number of LEDs	2, 4
Number of detectors in ADR	3, 4, 5, 6
Semi-angle at half power of LED	60°
Average output optical power	10 W
Modulation index	0.3
Gain of filter	0.9
Refractive index of concentrator	1.5
Radius of detector	2.5 mm
Gap between top and side detectors	3 mm
Responsivity of detector	0.53 A/W
Modulation bandwidth	10 MHz
Background current	5100 μA
Number of users	121

IV. RESULTS AND DISCUSSIONS

In this section, we evaluate the performance of an indoor multi-cell VLC system using the proposed generalized ADR. The multi-cell VLC system is configured in a 5 m × 5 m × 3 m room, where the height of the receiving plane is 0.85 m. The coordinates of the lower left corner of the floor are set to (0, 0, 0) and the units of all the coordinates are meters. As illustrated in Fig. 4, two LED layouts with $N_t = 2$ and 4 are considered. For $N_t = 2$, the coordinates of two LEDs are (1.25, 2.5, 3) and (3.75, 2.5, 3). For $N_t = 4$, the coordinates of four LEDs are (1.25, 1.25, 3), (1.25, 3.75, 3), (3.75, 3.75, 3) and (3.75, 1.25, 3). The key parameters of the multi-cell VLC system are listed in Table I. The semi-angle at half power, the average output optical power and the modulation index of each LED are 60°, 10 W and 0.3, respectively. The gain of the optical filter is 0.9. The refractive index of the optical concentrator is 1.5. The radius of all the circular-shaped detectors is 2.5 mm, corresponding to an active area of 19.6 mm^2. The gap between the top detector

$$\lambda_{i,MRC} = \frac{\left(\sum_{j=1}^{N_r} \omega_{ij}\gamma\xi h'_{ij} P_0\right)^2}{\sum_{j=1}^{N_r}\left(\sum_{i'=1,\, i'\neq i}^{N_t} \left(\omega_{ij}\gamma\xi h'_{i'j} P_0\right)^2 + \omega^2_{ij}(\sigma^2_{j,\,shot} + \sigma^2_{j,\,thermal})\right)}. \tag{18}$$

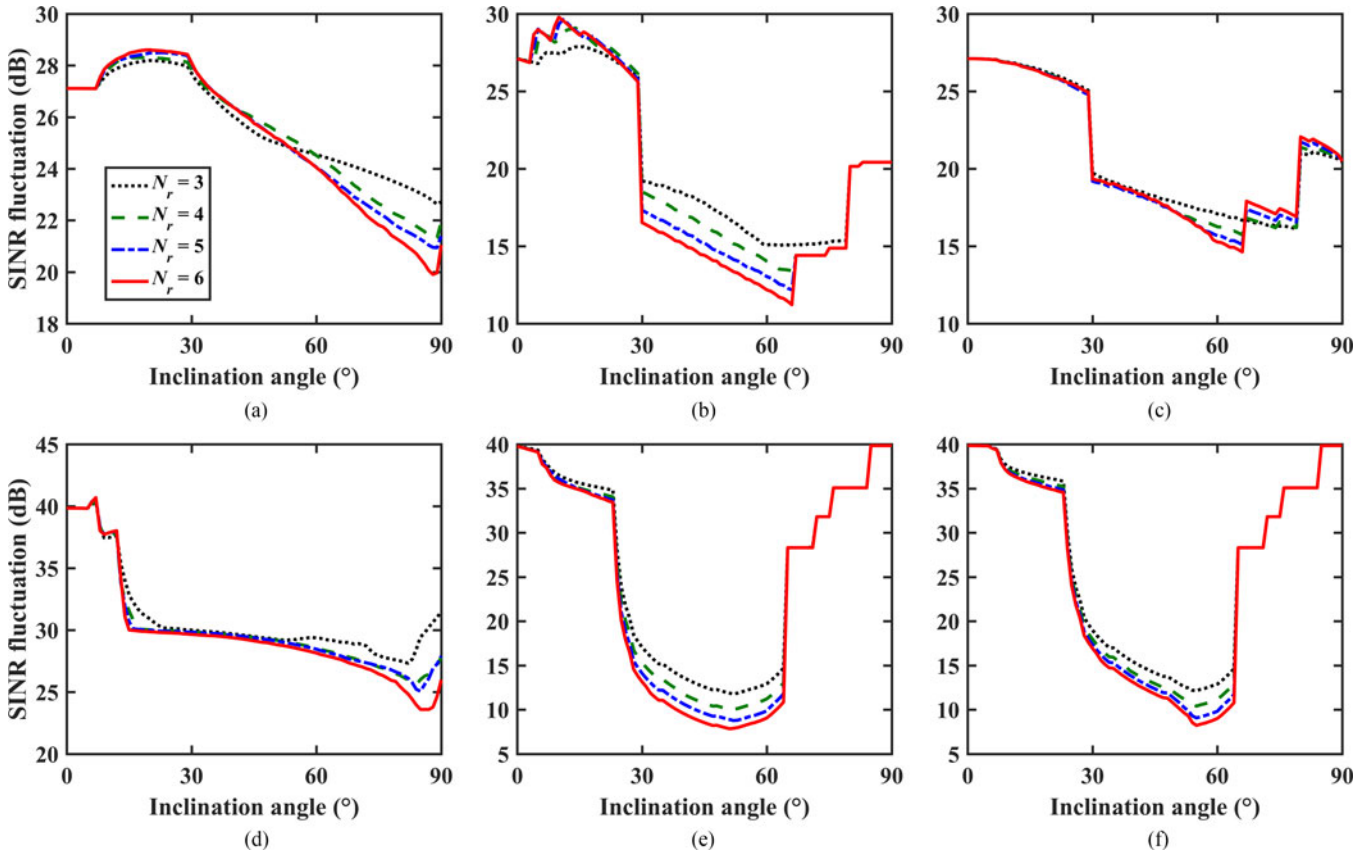

Fig. 5. SINR fluctuation vs. the inclination angle of the side detectors in the generalized ADR with different N_r values for (a) $N_t = 2$ with EGC, (b) $N_t = 2$ with SBC, (c) $N_t = 2$ with MRC, (d) $N_t = 4$ with EGC, (e) $N_t = 4$ with SBC, and (f) $N_t = 4$ with MRC.

and the side detectors is 3 mm. The responsivity of all detectors is 0.53 A/W. A modulation bandwidth of 10 MHz is used. The background current is 5100 μA due to the ambient light. To make sure that the generalized ADR can successfully receive the signal from at least one LED, the half-angle FOVs of the detectors are set to 60° and 45° for $N_t = 2$ and 4, respectively. It is assumed that there are totally 121 users in the multi-cell VLC system, which are uniformly distributed around the receiving plane, and the SINR fluctuation can be obtained by using (20).

It can be seen from (15) that the optical channel gain of each side detector is a function of the inclination angle ϕ, and hence the SINR fluctuation as defined in (20) is also a function of the inclination angle ϕ. Fig. 5 shows the relationship between the SINR fluctuation and the inclination angle ϕ for different numbers of LEDs ($N_t = 2, 4$), different numbers of detectors ($N_r = 3, 4, 5, 6$) and different diversity combining techniques (EGC, SBC, MRC). For $N_t = 2$, as shown in Figs. 5(a)–(c), the SINR fluctuation using EGC is relatively high and the minimum value is 19.9 dB with $N_r = 6$ and an inclination angle of 88°. However, when SBC or MRC is adopted, the SINR fluctuation can be greatly reduced. More specifically, the minimum SINR fluctuations are 11.2 and 14.6 dB when using SBC and MRC, respectively, both with $N_r = 6$ and an inclination angle of 66°. For $N_t = 4$, as shown in Figs. 5(d)–(f), it is similar that high SINR fluctuations are obtained when using EGC, which can be substantially reduced when SBC or MRC is adopted. For all N_r values, the optimal inclination angles to achieve the minimum SINR fluctuations when using SBC and MRC are 51° and 55°, respectively. Therefore, the SINR fluctuation can be minimized by selecting a proper diversity combining technique, a suitable number of detectors and an optimal inclination angle.

Using the obtained optimal inclination angles, Fig. 6 shows the achievable minimum SINR fluctuation versus the number of detectors in the optimized ADR. For $N_t = 2$, as shown in Fig. 6(a), the minimum SINR fluctuation is gradually reduced with the increased number of detectors in the optimized ADR. The highest SINR fluctuations are obtained when using EGC, which is because all the output signals are simply added together with the same weights and the interference might not be efficiently suppressed [29]. Furthermore, the minimum SINR fluctuation achieved by using SBC is much lower than MRC, especially when N_r is relatively large. For example, a 3.4-dB reduction of minimum SINR fluctuation is attained by SBC in comparison to MRC when $N_r = 6$. However, for $N_t = 4$, as shown in Fig. 6(b), SBC only slightly outperforms MRC. For example, when $N_r = 6$, the minimum SINR fluctuations are 7.9 and 8.2 dB for SBC and MRC, respectively, indicating a difference of only 0.3 dB.

Fig. 7 compares the average SINR distributions over the receiving plane using a single-element receiver (SER), i.e., only the top detector, and the optimized ADR with SBC. As we can see, for both $N_t = 2$ and 4, the SINR fluctuates greatly due to

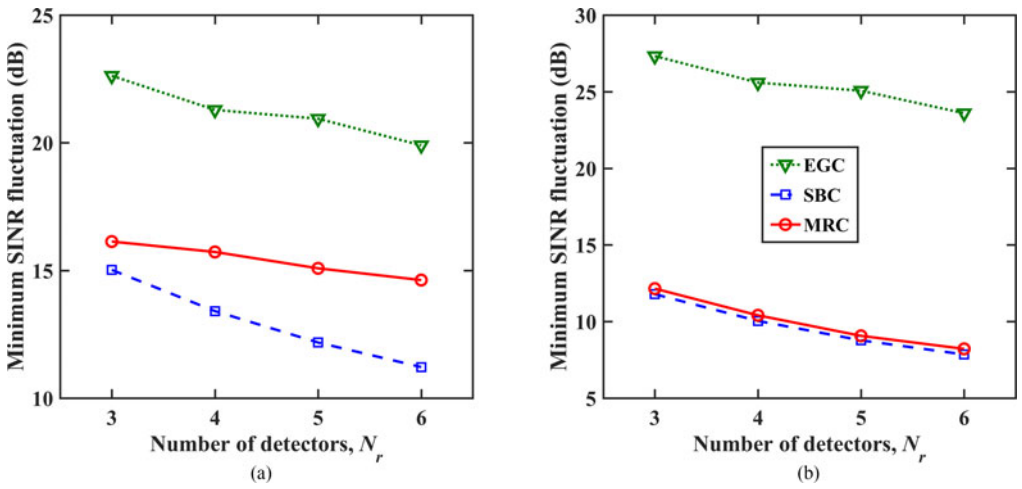

Fig. 6. Minimum SINR fluctuation vs. the number of detectors in the optimized ADR using different diversity combining techniques for (a) $N_t = 2$ and (b) $N_t = 4$.

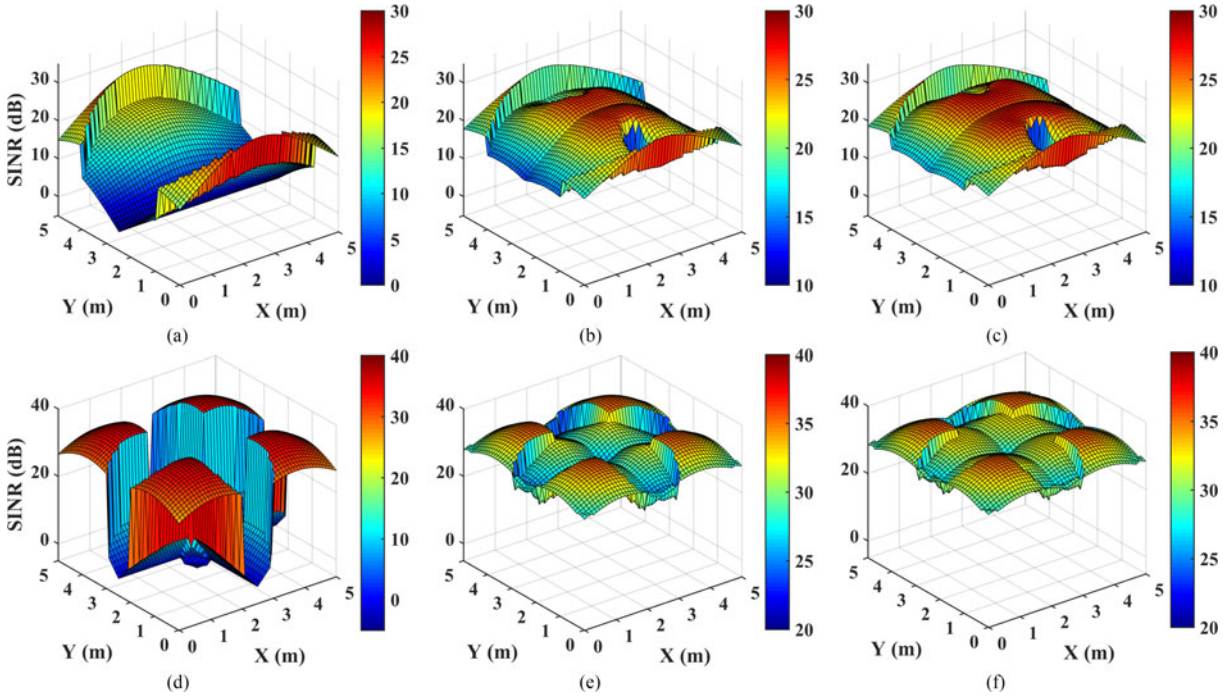

Fig. 7. Average SINR distribution over the receiving plane using SER and optimized ADR with SBC: (a) $N_t = 2$, SER, (b) $N_t = 2$, ADR with $N_r = 4$, (c) $N_t = 2$, ADR with $N_r = 6$, (d) $N_t = 4$, SER, (e) $N_t = 4$, ADR with $N_r = 4$, and (f) $N_t = 2$, ADR with $N_r = 6$.

the severe ICI when using the SER. SINR value is even below 0 dB at the symmetrical positions, e.g., Y = 2.5 m for $N_t = 2$, and X = 2.5 m and Y = 2.5 m for $N_t = 4$. The SINR fluctuations reach 27.1 and 40.3 dB for $N_t = 2$ and 4, respectively. However, by using the optimized ADR, the average SINR distributions are much more flat and the SINR fluctuations are significantly reduced. When the number of the detectors is increased from 4 to 6, the SINR fluctuations can be further reduced.

V. Conclusion and Future Work

In this paper, we have proposed and evaluated a generalized ADR structure for SINR fluctuation reduction in indoor multi-cell VLC systems. Different diversity combining techniques are applied in the generalized ADR and the impact of receiver random rotation is also considered. It has been shown by the numerical results that the SINR fluctuation of an indoor multi-cell VLC system using the generalized ADR largely depends on the inclination angle of all the side detectors. By selecting an optimal inclination angle, the SINR fluctuation around the receiving plane can be minimized. In our numerical study, two LED layouts ($N_t = 2, 4$), three diversity combining techniques (EGC, SBC and MRC) and four different numbers of detectors in the optimized ADR ($N_r = 3, 4, 5, 6$) are evaluated in a typical room. The obtained results verify that the SINR fluctuation over the receiving plane can be gradually reduced when

the number of detectors in the optimized ADR is increased from 3 to 6, for both $N_t = 2$ and 4. It is further revealed that SBC is much more suitable than EGC and MRC for the optimized ADR when $N_t = 2$. Specifically, a minimum SINR fluctuation reduction of 3.4 dB is achieved by using SBC compared with MRC when $N_t = 2$ and $N_r = 6$. In contrast, nearly the same SINR fluctuations can be obtained for SBC and MRC when $N_t = 4$ for all N_r values. Applying the optimized ADR based on SBC with $N_r = 6$, the SINR fluctuations are reduced from 27.1 and 40.3 dB to 11.2 and 7.9 dB, indicating SINR fluctuation reductions of 15.9 and 32.4 dB, for $N_t = 2$ and 4, respectively. In conclusion, the proposed optimized ADR has great potential for SINR fluctuation reduction in indoor multi-cell VLC systems.

In this work, only LOS transmission is considered while the interference effects caused by signal reflections due to NLOS transmission is neglected. In our future work, we will consider the impact of signal reflections on the performance of indoor multi-cell VLC systems using the generalized ADR. Moreover, the impact of random tilting of the ADR will also be analyzed.

ACKNOWLEDGMENT

This work was conducted within the Delta-NTU Corporate Lab for Cyber-Physical Systems.

REFERENCES

[1] T. Baumgartner, F. Wunderlich, A. Jaunich, T. Sato, and G. Bundy, "Lighting the way: Perspectives on the global lighting market," McKinsey Co., Nashua, NH, USA, Tech. Rep., 2012. [Online]. Available: http://www.ledsmagazine.com/articles/2011/08/mckinseyreleases-lighting-market-report.html

[2] T. Komine and M. Nakagawa, "Fundamental analysis for visible-light communication system using LED lights," *IEEE Trans. Consum. Electron.*, vol. 50, no. 1, pp. 100–107, Feb. 2004.

[3] S. Arnon, Ed., *Visible Light Communication*. Cambridge, U.K.: Cambridge Univ. Press, 2015.

[4] H. Haas, L. Yin, Y. Wang, and C. Chen, "What is LiFi?," *J. Lightw. Technol.*, vol. 34, no. 6, pp. 1533–1544, Mar. 2016.

[5] H. Haas, "Visible light communication," in *Proc. Opt. Fiber Commun. Conf.*, Mar. 2015, Paper Tu2G.5.

[6] J. Armstrong, Y. Sekercioglu, and A. Neild, "Visible light positioning: A roadmap for international standardization," *IEEE Commun. Mag.*, vol. 51, no. 12, pp. 68–73, Dec. 2013.

[7] P. Pathak, X. Feng, P. Hu, and P. Mohapatra, "Visible light communication, networking, and sensing: A survey, potential and challenges," *IEEE Commun. Surveys Tuts.*, vol. 17, no. 4, pp. 2047–2077, Nov. 2015.

[8] D. H. Wu, W.-D. Zhong, Z. Ghassemlooy, and C. Chen, "Short-range visible light ranging and detecting system using illumination light emitting diodes," *IET Optoelectron.*, vol. 10, no. 3, pp. 94–99, Jun. 2016.

[9] Z. Ghaseemlooy, W. Popoola, and S. Rajbhandri, *Optical Wireless Communications, System and Channel Modelling With MATLAB*. London, U.K.: CRC Press, Aug. 2012.

[10] C. Chen, W.-D. Zhong, and D. H. Wu, "Indoor OFDM visible light communications employing adaptive digital pre-frequency domain equalization," in *Proc. Conf. Lasers and Electro-Opt.*, Jun. 2016, Paper JTh2A.118.

[11] H. Minh *et al.*, "100-Mb/s NRZ visible light communications using a post-equalized white LED," *IEEE Photon. Technol. Lett.*, vol. 21, no. 15, pp. 1063–1065, Aug. 2009.

[12] S. Hashemi, Z. Ghassemlooy, L. Chao, and D. Benhaddou, "Orthogonal frequency division multiplexing for indoor optical wireless communications using visible light LEDs," in *Proc. 6th Int. Symp. Commun. Syst. Netw. Digit. Signal. Process.*, Jul. 2008, pp. 174–178.

[13] C. Chen, W.-D. Zhong, and D. H. Wu, "Non-Hermitian symmetry orthogonal frequency division multiplexing for multiple-input multiple-output visible light communications," *J. Opt. Commun. Netw.*, vol. 9, no. 1, pp. 36–44, Jan. 2017.

[14] L. Zeng *et al.*, "High data rate multiple input multiple output (MIMO) optical wireless communications using white led lighting," *IEEE J. Sel. Areas Commun.*, vol. 27, no. 9, pp. 1654–1662, Dec. 2009.

[15] C. Chen, W.-D. Zhong, and D. H. Wu, "On the coverage of multiple-input multiple-output visible light communications [Invited]," *J. Opt. Commun. Netw.*, vol. 9, no. 9, pp. D31–D41, Sep. 2017.

[16] H. Marshoud, V. M. Kapinas, G. K. Karagiannidis, and S. Muhaidat, "Non-orthogonal multiple access for visible light communications," *IEEE Photon. Technol. Lett.*, vol. 28, no. 1, pp. 51–54, Jan. 2016.

[17] C. Chen, W.-D. Zhong, H. L. Yang, and P. F. Du, "On the performance of MIMO-NOMA-based visible light communication systems," *IEEE Photon. Technol. Lett.*, vol. 30, no. 4, pp. 307–310, Feb. 2018.

[18] C. Chen, D. Basnayaka, and H. Haas, "Downlink performance of optical attocell networks," *J. Lightw. Technol.*, vol. 34, no. 1, pp. 137–156, Jan. 2016.

[19] H. L. Yang, C. Chen, and W.-D. Zhong, "Cognitive multi-cell visible light communication with hybrid underlay/overlay resource allocation," *IEEE Photon. Technol. Lett.*, vol. 30, no. 12, pp. 1135–1138, Jun. 2018.

[20] H. Kim, D. Kim, S. Yang, Y. Son, and S.-K. Han, "Mitigation of inter-cell interference utilizing carrier allocation in visible light communication system," *IEEE Commun. Lett.*, vol. 16, no. 4, pp. 526–529, Apr. 2012.

[21] S.-Y. Jung, D.-H. Kwon, S.-H. Yang, and S.-K. Han, "Inter-cell interference mitigation in multi-cellular visible light communications," *Opt. Exp.*, vol. 24, no. 8, pp. 8512–8526, Apr. 2016.

[22] D. Bykhovsky and S. Arnon, "Multiple access resource allocation in visible light communication systems," *J. Lightw. Technol.*, vol. 32, no. 8, pp. 1594–1600, Apr. 2014.

[23] H.-N. Ryoo, D.-H. Kwon, S.-H. Yang, and S.-K Han, "Differential optical detection in VLC for inter-cell interference reduced flexible cell planning," *IEEE Photon. Technol. Lett.*, vol. 28, no. 23, pp. 2728–2731, Dec. 2016.

[24] A. Burton, Z. Ghassemlooy, S. Rajbhandari, and S.-K. Liaw, "Design and analysis of an angular-segmented full-mobility visible light communications receiver," *Trans. Emerg. Telecommun. Technol.*, vol. 25, no. 6, pp. 591–599, Jun. 2014.

[25] A. Nuwanpriya, S. Ho, and C. S. Chen, "Indoor MIMO visible light communications: Novel angle diversity receivers for mobile users," *IEEE J. Sel. Areas Commun.*, vol. 33, no. 9, pp. 1780–1792, Sep. 2015.

[26] C. Chen, W.-D. Zhong, D. Wu, and Z. Ghassemlooy, "Wide-FOV and high-gain imaging angle diversity receiver for indoor SDM-VLC systems," *IEEE Photon. Technol. Lett.*, vol. 28, no. 19, pp. 2078–2081, Oct. 2016.

[27] C. He, T. Q. Wang, and J. Armstrong, "Performance of optical receivers using photodetectors with different fields of view in a MIMO ACO- OFDM system," *J. Lightw. Technol.*, vol. 33, no. 23, pp. 4957–4967, Dec. 2015.

[28] K. Ajit and S. K. Ghorai, "Reduction of channel correlation for multiuser-MIMO system in visible light communications," in *Proc. IEEE Int. Conf. Signal Process. Commun.*, Dec. 2016, pp. 22–25.

[29] Z. Cheng, N. Serafimovski, and H. Haas, "Angle diversity for an indoor cellular visible light communication system," in *Proc. Veh. Technol. Conf. Spring*, May 2014, pp. 1–5.

[30] Z. Chen, D. Tsonev, and H. Haas, "Improving SINR in indoor cellular visible light communication networks," in *Proc. IEEE Int. Conf. Commun.*, Jun. 2014, pp. 3383–3388.

[31] W.-D. Zhong, C. Chen, H. L. Yang, and P. F. Du, "Performance analysis of angle diversity multi-element receiver in indoor multi-cell visible light communication systems," in *Proc. Int. Conf. Transparent Opt. Netw.,* Jul. 2017, Paper Mo.D2.2.

[32] Z. X. Wang, C. Y. Yu, W.-D Zhong, J. Chen, and W. Chen, "Performance of a novel LED lamp arrangement to reduce SNR fluctuation for multi-user visible light communication systems," *Opt. Exp.*, vol. 20, pp. 4564–4573, Feb. 2012.

[33] P. Mmbaga, J. Thompson, and H. Haas, "Performance analysis of indoor diffuse VLC MIMO channels using angular diversity detectors," *J. Lightw. Technol.*, vol. 34, no. 4, pp. 1254–1266, Feb. 2016.

[34] C. Edwards and D. Penney, *Calculus*. Englewood Cliffs, NJ, USA: Prentice Hall, 2002.

[35] Z. X. Wang, C. Y. Yu, W.-D. Zhong, and J. Chen, "Performance improvement by tilting receiver plane in M-QAM OFDM visible light communications," *Opt. Exp.*, vol. 19, no. 14, pp. 13418–13427, Jul. 2011.

[36] D. G. Brennan, "Linear diversity combining techniques," *Proc. IEEE*, vol. 91, no. 2, pp. 331–356, Feb. 2003.

Authors biographies not available at the time of publication.